NANO LETTERS

Concept of Lattice Mismatch and Emergence of Surface States in Two-dimensional Hybrid Perovskite Quantum Wells

Mikaël Kepenekian,*,[†] Boubacar Traore,[†] Jean-Christophe Blancon,[‡] Laurent Pedesseau,[¶] Hsinhan Tsai,[‡,§] Wanyi Nie,[‡] Constantinos C. Stoumpos,[∥] Mercouri G. Kanatzidis,[∥] Jacky Even,[¶] Aditya D. Mohite,[‡] Sergei Tretiak,*,[‡] and Claudine Katan*,[†]

[†]Univ Rennes, ENSCR, INSA Rennes, CNRS, ISCR−UMR 6226, F-35000 Rennes, France
[‡]Los Alamos National Laboratory, Los Alamos, New Mexico 87545, United States
[¶]Univ Rennes, INSA Rennes, CNRS, FOTON−UMR 6082, F-35000 Rennes, France
[§]Department of Materials Science and Nanoengineering, Rice University, Houston, Texas 77005, United States
[∥]Department of Chemistry, Northwestern University, Evanston, Illinois 60208, United States

Ⓢ *Supporting Information*

ABSTRACT: Surface states are ubiquitous to semiconductors and significantly impact the physical properties and, consequently, the performance of optoelectronic devices. Moreover, surface effects are strongly amplified in lower dimensional systems such as quantum wells and nanostructures. Layered halide perovskites (LHPs) are two-dimensional solution-processed natural quantum wells where optoelectronic properties can be tuned by varying the perovskite layer thickness n, i.e., the number of octahedra spanning the layer. They are efficient semiconductors with technologically relevant stability. Here, a generic elastic model and electronic

structure modeling are applied to LHPs heterostructures with various layer thickness. We show that the relaxation of the interface strain is triggered by perovskite layers above a critical thickness. This leads to the release of the mechanical energy arising from the lattice mismatch, which nucleates the surface reorganization and may potentially induce the formation of previously observed lower energy edge states. These states, which are absent in three-dimensional perovskites are anticipated to play a crucial role in the design of LHPs for optoelectronic systems.

KEYWORDS: *Halide perovskites, layered materials, lattice mismatch, surface states, exciton, density functional theory*
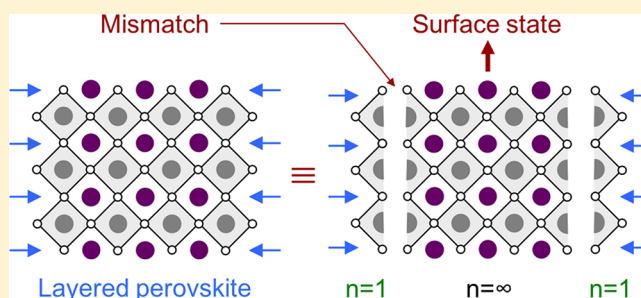
Surfaces and interfaces are known to play a central part in the performances of classical semiconductor based devices.[1−3] This holds true for the recently emerged halide perovskites.[4,5] The two-dimensional (2D) members of the family, layered halide perovskites (LHPs), are 2D solution-processed natural quantum wells[6−8] and present superior photo- and chemostability compared to their three-dimensional (3D) counterparts. They show strong promise in high performance optoelectronic devices such as photovoltaics, field effect transistors, electrically injected light emission, and polarized optical spin injection.[9−14] Their properties depend on the number n of MX_6 octahedra that span the perovskite layer (M is a metal, X is a halogen). As in classical semiconductors,[2] surface and interface structures can have a strong influence on the properties of LHPs.[15] While experimental results exist, especially in Ruddlesden−Popper perovskites (RPPs) of general formula $A'_2A_{n-1}M_nX_{3n+1}$ (A and A′ being cations), there is no simple model to predict and control LHP surface properties.

Here, we design a model based on the concept of lattice mismatch, considering LHPs as heterostructures built from the $n = 1$ monolayered perovskite A'_2MX_4 and the $n = \infty$ 3D AMX_3. The capacities of the model are first examined taking the RPPs of the general formula $(BA)_2(MA)_{n-1}Pb_nI_{3n+1}$. This specific family of RPPs is further inspected by means of DFT atomistic calculations, showing that their optical properties are decisively impacted by surface relaxations occurring for structures with $n > 2$. The general picture that emerges from the combined study leads to understanding of physical phenomena underpinning surface reconstruction and concomitant modifications of electronic structure, and allows to formulate the design principles of LHP materials optimized for optoelectronics, solid-state lighting, or photovoltaics.

It has been shown earlier that ordered LHPs structures can be treated as composite L1/L2 systems with coherent interfaces, although the definition of the L1 and L2 bulk materials must be chosen with care.[16] Such a framework allows
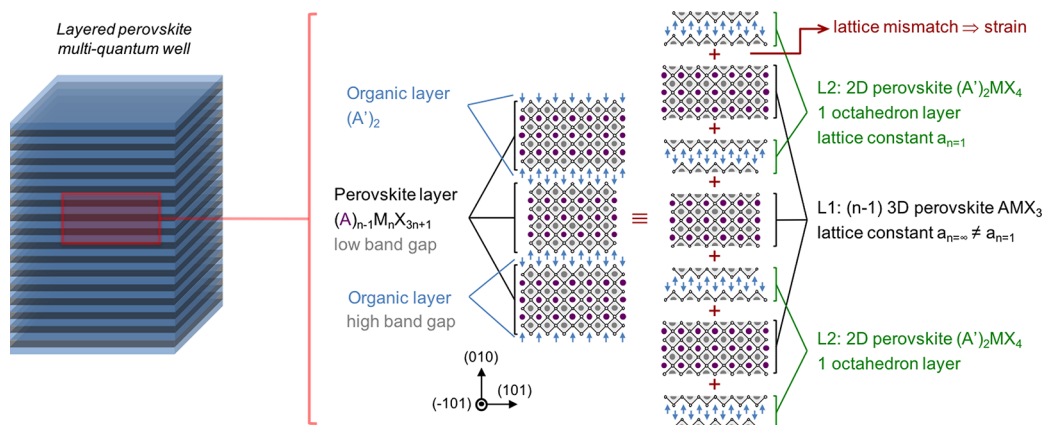
Figure 1. Schematics of hybrid layered compounds regarded as heterostructures L1/L2 with L1 the 3D ($n = \infty$) bulk material, e.g., MAPbI$_3$, and L2, a $n = 1$ compound, e.g., $(BA)_2PbI_4$.
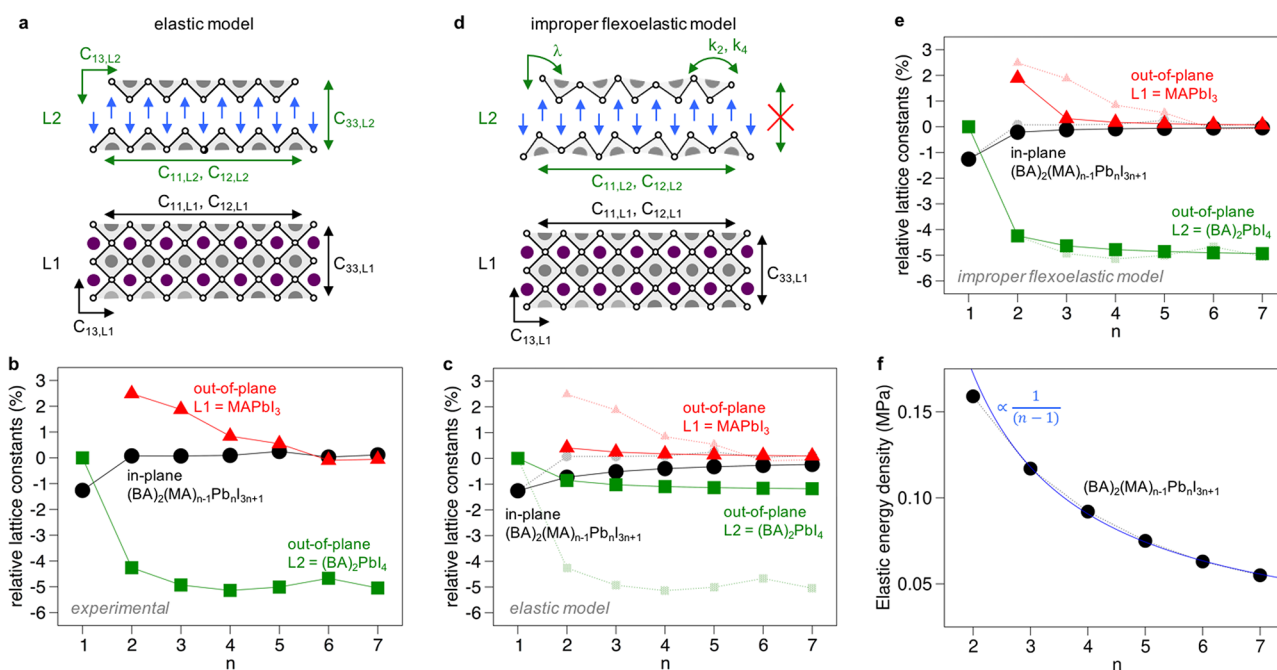

Figure 2. (a) Parameters of the purely elastic model, relying on the strain tensor $\{C_{ij}\}$. (b) In-plane expansion and out-of-plane contractions of experimental lattice constants for $(BA)_2(MA)_{n-1}Pb_nI_{3n+1}$ and the L1 and L2 layers. The room-temperature structures of MAPbI$_3$ and $(BA)_2PbI_4$ serve as references for L1 and L2 structures, respectively. (c) Same from the purely elastic model. (d) Parameters of the improper flexoelastic model. L2 now react to the strain by also modifying the in-plane and out-of-plane tilting angles through λ, k_2 and k_4 (see text and Text I, SI). (e) Same as (b) from the improper flexoelastic model (see SI for details). (f) Computed elastic energy density for the $(BA)_2(MA)_{n-1}Pb_nI_{3n+1}$ heterostructure (black circles). Nonlinear fit related to the ratio between the volume occupied by L2 (1) and L1 ($n - 1$) layers in the L1/L2 heterostructure leading to a $1/(n - 1)$ behavior.

relevant analysis of electronic and dielectric properties of the composite.[16,17] To investigate mechanical properties, we construct a model (see Text I, Supporting Information (SI) for details) based on the theory of elasticity in classical semiconductor heterostructures[18] by identifying the LHP structure with a multiquantum well system (Figure 1) with alternating stacking of 3D perovskite layers L1 (AMX$_3$, of thickness $n - 1$) and of 2D perovskite monolayers L2 (single octahedron, $n = 1$). This combination forms an interface between two structurally different layers, equivalent to a so-called L1/L2 heterostructure with a coherent interface (lattices are continuous across the interface in two directions).[19]

A first simple approach may be inspired by the elastic model used to predict the influence of lattice mismatch during epitaxial growth of conventional semiconductor heterostructures.[18,19] For an epitaxial layer with a low lattice mismatch ($\epsilon_{11} = \epsilon_{22}$) and the condition for a free (001) surface ($\sigma_{33} = 0$) on a rigid (001) zinc-blende substrate, the relation between stress and strain tensors (with C_{ij} the components of the tensor) leads to the out-of-plane strain $\epsilon_{33} = (-2C_{12}\epsilon_{11})/C_{11}$. Alternatively, the same result can be obtained by minimizing the elastic free energy with respect to ϵ_{33}. This model must be adapted for LHPs. The elastic properties of both L1 and L2 layers must be taken into account with ϵ_{ij} transforming to $\epsilon_{ij,L1}$ and $\epsilon_{ij,L2}$ and C_{ij} to $C_{ij,L1}$ and $C_{ij,L2}$ (Figure 2a). Considering the transverse elastic approximation for L1 $= (n - 1)$AMX$_3$, then the total elastic energy of the L1/L2 composite heterostructure is given by
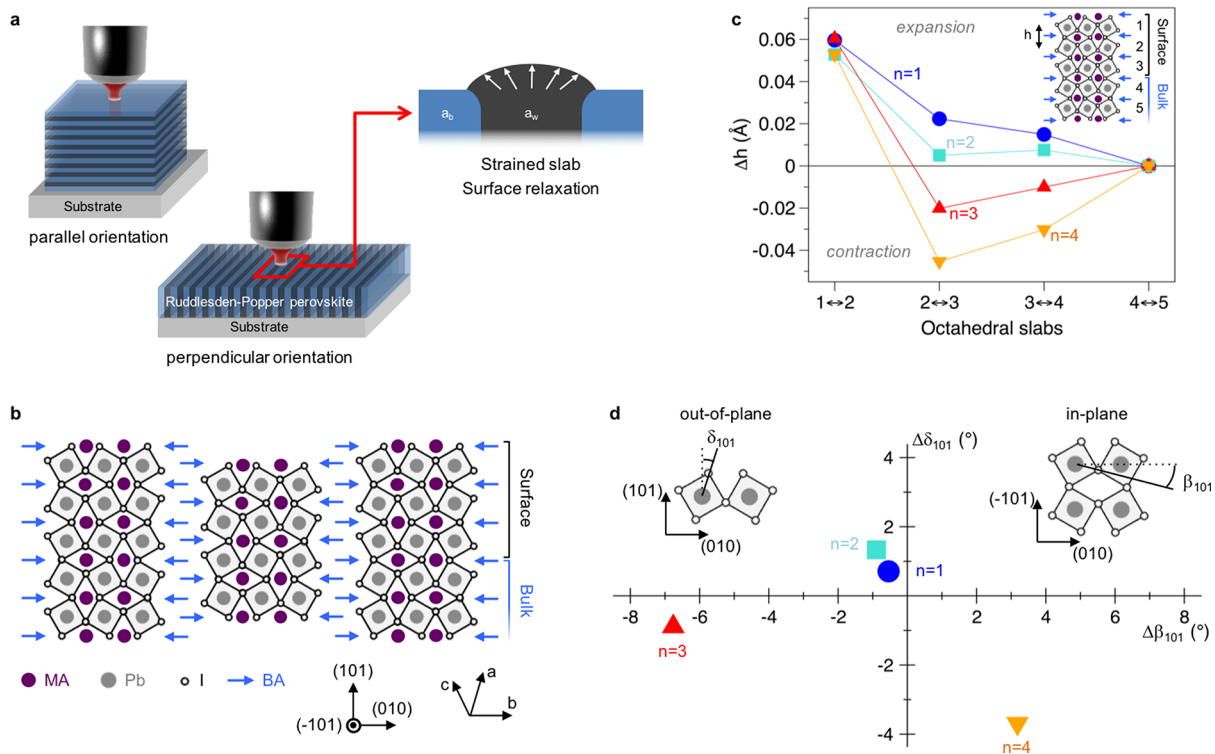
Figure 3. Surface relaxation in LHP multiquantum wells. (a) Schematics of LHP-based devices in parallel and perpendicular orientation. (b) Schematics of the (101) surface of the layered perovskite $(BA)_2(MA)_{n-1}Pb_nI_{3n+1}$ with $n = 3$. (c) Variation of the interlayer height difference (Δh) from bulk-like to surface (see inset). (d) Variation of in-plane (β_{101}) and out-of-plane (δ_{101}) tiltings of surface octahedra due to the (101) surface relaxation.

$$F = \frac{1}{2}Sl_{L1}[C_{11,L1}(\epsilon_{11,L1}^2 + \epsilon_{22,L1}^2 + \epsilon_{33,L1}^2)$$
$$+ 2C_{12,L1}(\epsilon_{11,L1}\epsilon_{22,L1} + \epsilon_{11,L1}\epsilon_{33,L1} + \epsilon_{22,L1}\epsilon_{33,L1})]$$
$$+ \frac{1}{2}Sl_{L2}[C_{11,L2}(\epsilon_{11,L2}^2 + \epsilon_{22,L2}^2) + C_{33,L2}\epsilon_{33,L2}^2$$
$$+ 2C_{12,L2}\epsilon_{11,L2}\epsilon_{22,L2} + 2C_{13,L2}(\epsilon_{11,L2}\epsilon_{33,L2}$$
$$+ \epsilon_{22,L2}\epsilon_{33,L2})] \tag{1}$$

where S is the surface of the coherent interface, $l_{L1} = (n - 1)c_{3D}$ and $l_{L2} = c_{2D}$ are the thicknesses of the two layers, and c_{2D} and c_{3D} are the stacking parameters of $(A')_2MX_4$ and AMX_3, respectively. Considering that the two layers share the same in-plane lattice parameter a and the conditions for free strain relaxation along the stacking axis, the equilibrium in-plane lattice parameter a_{eq} is derived by minimizing the total energy, yielding

$$a_{eq} = \frac{\frac{K_{L1}}{a_{3D}} + \frac{K_{L2}}{a_{2D}}}{\frac{K_{L1}}{a_{3D}^2} + \frac{K_{L2}}{a_{2D}^2}} \tag{2}$$

with

$$K_{L1} = (n - 1)c_{3D}\left(C_{11,L1} + C_{12,L1} - 2\frac{C_{12,L1}^2}{C_{11,L1}}\right)$$

and

$$K_{L2} = c_{2D}\left(C_{11,L2} + C_{12,L2} - 2\frac{C_{13,L2}^2}{C_{33,L2}}\right)$$

To illustrate this general concept, we consider the family of RPPs of general formula $(BA)_2(MA)_{n-1}Pb_nI_{3n+1}$ that can be synthesized in phase-pure form (only one n value).[20−22] It can be approximated to an $L1/L2$ heterostructure with $L1 = (n-1)MAPbI_3$ and $L2 = (BA)_2PbI_4$ (Figure 1). Figure 2b represents experimentally observed variations of the in-plane average lattice parameter (perpendicular to the stacking axis of the LHP, i.e., to (010)) as a function of n for the native $(BA)_2(MA)_{n-1}Pb_nI_{3n+1}$ heterostructure, as well as the out-of-plane lattice parameters (along the stacking axis of the LHP) for the end members of the homologous series $L1$ $((n-1)MAPbI_3)$ and $L2$ $(n = 1, (BA)_2PbI_4)$. As qualitatively predicted based on elasticity (Figure 2c), the in-plane lattice expansion from $n = 1$ to $n = \infty$ gives rise to an out-of-plane lattice contraction in both $L1$ and $L2$ layers. However, the experimental variation of the in-plane parameter is noticeably steep, the in-plane parameter of MAPbI$_3$ ($n = \infty$) being almost already recovered for $n = 2$. A similar steep variation is observed for the out-of-plane lattice parameter of the L2 layer. The deficiency of a pure elastic model (Figure 2c) can be traced back to additional rotational degrees of freedom, namely, octahedral tilting, which also afford a path to relax the accumulated mechanical energy (Figure 2d). In fact, quantitative agreement between experimental results (Figure 2b) and model predictions (Figure 2e) can only be obtained when considering that $L1$ reacts in a purely elastic manner, whereas $L2$ relaxes the strain through the variation of octahedra tilt angles (Figure 2d). This can be observed on the angles extracted from the $(BA)_2(MA)_{n-1}Pb_nI_{3n+1}$ RPP experimental structures (see Text II, Figure S1, and Table S1, SI). The octahedra tilt angles in $L2$ structure are indeed more important than in the $L1$ layers. In other words, the mechanical
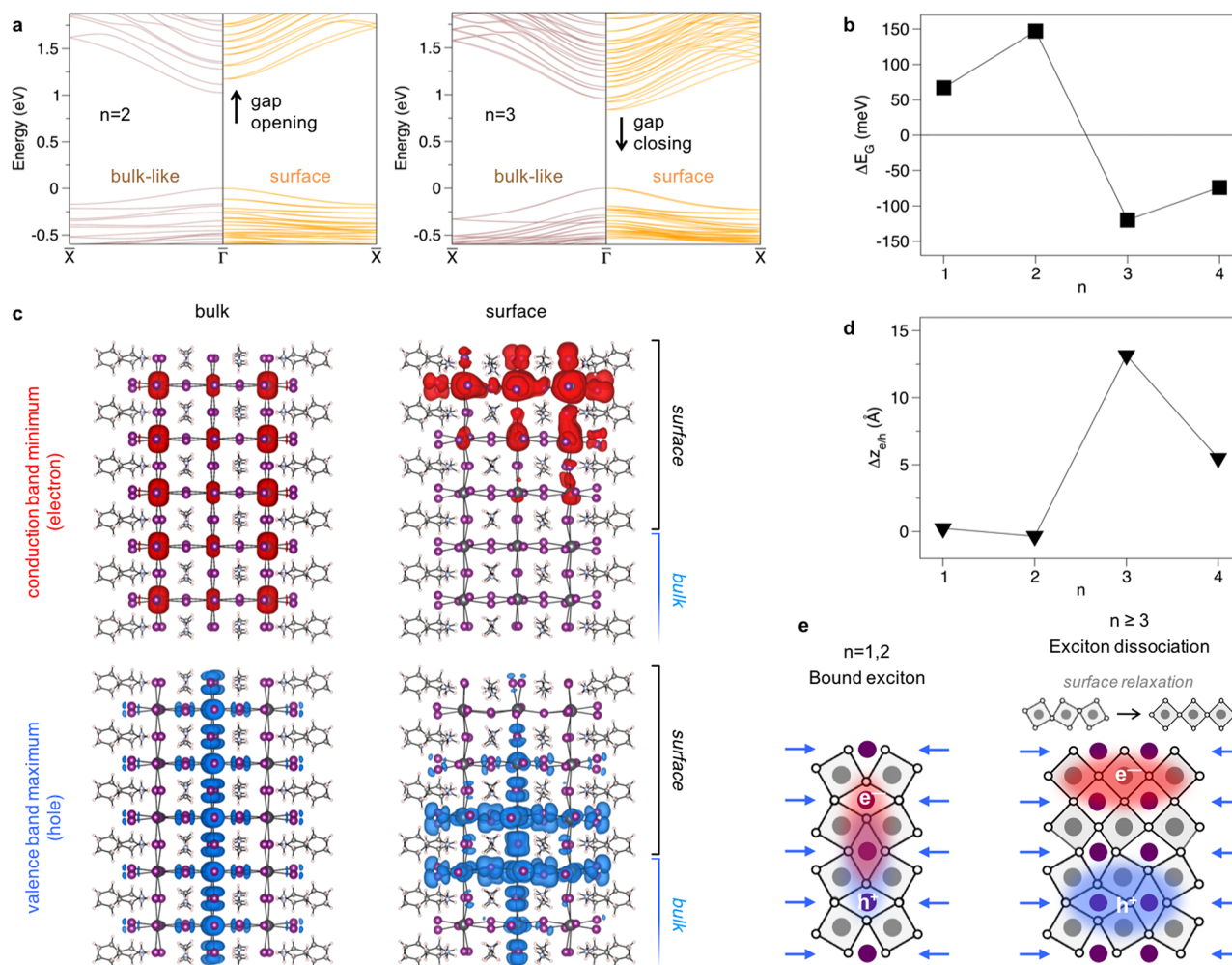
Figure 4. Impact of surface structural relaxation on electronic and optical properties in $(BA)_2(MA)_{n-1}Pb_nI_{3n+1}$. (a) Slab band structures in the bulk-like (left) and relaxed (101) surface (right) for $n = 2$ and 3. (b) DFT variation of E_G going from bulk-like to relaxed (101) surface. (c) Partial charge densities computed at the valence band maximum and conduction band minimum for the $n = 3$ RPP in bulk and relaxed surface. (d) Difference between the barycenter of electron and hole wave functions. (e) Schematics of the surface-induced exciton dissociation in RPPs with $n \geqslant 3$.

energy is more efficiently relaxed in the bulk RPPs structures by rotation of those octahedra that are directly in contact with the flexible organic cations, than by Pb–I bond elongation.

Classic theory of elasticity predicts that, for a heterostructure L1/L2 with a large lattice mismatch between L1 and L2, the structure may undergo a reorganization for a critical layer thickness, to form nanostructures at the surface in order to relax the accumulated bulk mechanical energy.[19] From the above results, the elastic energy density in RPPs with varying perovskite thickness n was computed (Figure 2f). We observed a maximum elastic energy density of ∼0.16 MPa for the RPP $n = 2$, and a monotonic reduction of this energy with increasing n, which ultimately vanishes for bulk 3D perovskite ($n \rightarrow \infty$). The monotonic decrease of elastic energy density is related to the behavior of lattice constants. From Figure 2f, one can see that starting from $n = 3$, L1 is defining the geometry, whereas L2 carries the stress in the heterostructure. As n grows, the ratio between L2 and L1 volumes decreases concomitantly with the elastic energy density although lattice parameters remain constants. Therefore, elastic energy density arising from the interface is expected to have direct consequences over surface properties for RPPs with low n values.

To gain microscopic insight of surface reorganization and their associate effect on physical properties, we further focus on the $(BA)_2(MA)_{n-1}Pb_nI_{3n+1}$ RPP ($n = 1-4$) using density functional theory (DFT). DFT allows modeling the structural relaxation at the relevant surfaces with account of all structural distortions (see Methods for computational details). Applications using RPPs as active materials mainly employ two different orientations; the 2D layers are either parallel or perpendicular to the substrate or an interface layer (Figure 3a). The most relevant surface of the RPP is then the (101) surface (Figure 3b),[9,15] which we model here on specifically designed slabs (Text III and Figure S3, SI), labeled as bulk-like and surface, for varying thickness $n = 1$ to 4. The calculated changes in the surface structure were represented by (i) the contraction/expansion of the octahedron slabs close to the surface in the (101) direction (Δ_h, Figure 3c), and (ii) the in-plane (β_{101}) and out-of-plane (δ_{101}) tilting of the octahedra close to the surface (Figure 3d).[7] This representation highlights our early conclusion drawn from the elastic model that the rotational degrees of freedom of the octahedra play an essential role in relaxing the internal elastic energy, in contrast with classical semiconductor descriptions where local strain
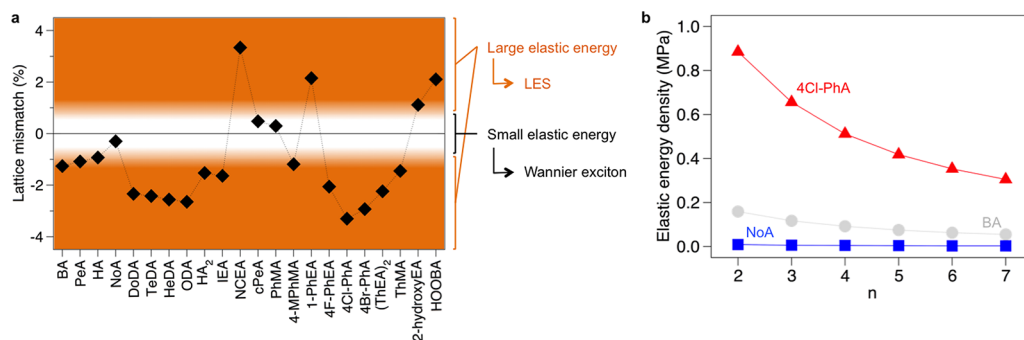
Figure 5. Design of LHPs for photovoltaics and optoelectronics. (a) Lattice mismatch between various monolayered A'_2PbI_4 perovskites ($n = 1$) and $MAPbI_3$ ($I4cm$; $n = \infty$). All data are taken from X-ray structures resolved at room-temperature. Names for organic compounds and corresponding references are given Table S4 (SI). (b) Computed elastic energy density for heterostructures built with $MAPbI_3$ and $(BA)_2PbI_4$ (gray line), $(C_9H_{19}NH_3)_2PbI_4$ (NoA, blue line), and $(4Cl-C_6H_4NH_3)_2PbI_4$ (4Cl-PhA, red line).

tensor suffices.[23] In an attempt to quantify the role of each degree of freedom, we have built a model allowing us to enforce contraction or elongation of bonds independently from octahedron tiltings (Figure S5, SI). Both mechanisms present similar contribution with a price of ca. 30 meV for a 1% strain on the structure.

Figure 3c shows the variation along the (101) direction of the distance h between octahedral slabs close to the perovskite surface. The reference value of h is obtained from the bulk-like region fixed in our DFT calculations ($4 \leftrightarrow 5$ distance in Figure 3c). The evolution of the interslab distance yields two opposite behaviors for $n = 1,2$ and $n > 2$. For $n > 2$, the surface slab expansion is accompanied by a contraction of the subsurface slabs, which leads to a decoupling of the top surface octahedron slab from the subsurface ones. However, for $n = 1,2$, expansion of octahedra slabs was observed in the entire surface region. A similar distinct behavior between $n = 1,2$ and $n > 2$ was noted by analyzing the surface relaxation in these BA-based RPPs occurring through in-plane and out-of-plane tilting of octahedra (Figure 3d). In fact, surface octahedra in $n = 1,2$ yield almost no rotational degrees of freedom, whereas $n > 2$ systems exhibit significantly larger tilting of surface octahedra. The drastic change of surface behavior, when increasing the perovskite layer thickness from $n = 2$ to $n = 3$ coincides with the appearance of specific signatures in the electronic structure of bulk RPP materials (Figure S4, SI). In particular, the Pb−I dangling bond located in the middle of the inorganic layer allows for a local strain relaxation (Figure S6, SI). The occurrence of a central octahedron, whose surrounding resembles the one in 3D perovskite, appears essential to trigger structural relaxation of the internal elastic energy.

We evaluate the impact of these surface relaxation processes on the electronic and optical properties of RRPs by comparing band structures and wave functions at the surface and in the bulk (Figure 4). The electronic band structure still presents a direct bandgap at the surface as compared to the bulk but with variation of the bandgap energy (Figure 4a,b; Figure S7, SI). We observe that the bandgap blueshifts by 70 and 150 meV for $n = 1$ and 2, respectively, and redshifts by 120 and 70 meV for $n = 3$ and 4, respectively. The accuracy of our approach is supported by (i) the excellent agreement between the calculated exciton properties in the bulk-like region with reported experimental results for the same materials (see detail in Text IV, SI),[24] and (ii) the similar pattern in the optical bandgap shift between the RPP layer surface with respect to

the bulk (Figure S8, SI).[15] According to surface relaxation results, lattice expansion at the (101) surface with relatively small octahedral tilting leads to a bandgap blueshift, whereas subsurface lattice compression with significant octahedral distortions results in a redshift of the bandgap due to appearance of in-gap electronic states.

In order to understand the microscopic impact of the structural changes at the surface on each type of charges, localized density of states (LDOS) have been integrated around the valence band maximum (hole) and conduction band minimum (electron), leading to partial charge densities (Figure 4c; Text V and Figure S9a,b, SI). For all n values, surface relaxation leads to hole wave functions repelled away from the surface to the bulk (Figure 4c, bottom panel). A similar behavior is observed for electrons for $n = 1,2$. In sharp contrast, for $n > 2$, the electron gets localized mainly at the top (101) surface slab (Figure 4c, top panel). Concomitantly, the preferential direction of electronic coupling switches from (010) to (101). From the barycenters of electron (z_e) and hole (z_h) partial charge density profiles (Figure S9c,d, SI), we inspect separation of carriers ($\Delta z_{e/h} = z_e - z_h$) and demonstrate that, upon appearance of in-gap states, the electron and hole get separated (Figure 4d). The effect is maximum for $n = 3$, $\Delta z_{e/h} = 13.2$ Å (5.5 Å for $n = 4$). Its impact on optical activity is estimated by computing Kane energies[25] for bulk-like and relaxed slabs (Text VI, SI). They reflect oscillator strengths of the optical-transitions and show a systematic reduction by 50%, 85%, 30%, and 95% for the four lowest excitations of $n = 3$ RPP (Table S3, SI). Such electron−hole separation at the surface is consistent with the longer photoluminescence lifetime of low-energy states reported recently.[15] To account for the excitonic properties of $(BA)_2(MA)_{n-1}Pb_nI_{3n+1}$, we further involve the semiempirical resolution of the Bethe−Salpeter equations including quantum and dielectric confinement as well as the overlap of electron and hole wave functions (Text IV, SI). The latter is essential for achieving quantitative agreement between the computed exciton binding energy and the low temperature spectroscopy results.[24] This can be intuited from the simplified screened electron−hole interaction (without dielectric confinement):

$$V_s(q_{\parallel}) = \frac{-e^2}{2\epsilon_w q_{\parallel}} \int\int \rho_e(z_e)\rho_h(z_h) \, e^{-q_{\parallel}|z_e - z_h|} \, dz_e dz_h \tag{3}$$

which shows that the separation of electrons and holes depicted in Figure 4c,d will cause the collapse of the exciton

binding energy (see Text VII and Figure S11, SI). Figure 4e summarizes our understanding of the formation of these low-energy states (LES) in BA-based RPPs with $n > 2$, which primarily stems from surface relaxation that strongly localizes the electron at the surface and facilitates dissociation of the strongly bound bulk exciton.

LES results from the release of the strain-induced elastic energy at the $L1/L2$ interface (Figure 2). From our elastic model, the amount of energy accumulated in the materials is directly dependent on the amplitude of lattice mismatch between layers in the heterostructure $L1/L2$, and as a result, tuning the LHP structure and composition can lead to drastic changes of surface properties. Using this general approach, the internal elastic energy density accumulated in the bulk of LHPs can be estimated for any composition and perovskite layer thickness. From a practical perspective, understanding the relaxation of the stored elastic energy at the surface of the LHP materials is of paramount importance and presents a perfect platform for the systematic and comprehensive evaluation and screening of LHP compounds with defined functionalities for novel devices. This concept is illustrated by changing organic cation A′ in RPPs (Figure 5a). For example, replacing BA with $C_9H_{19}NH_3$ (NoA), which has a significantly smaller lattice mismatch,[26] results in the reduction of the elastic energy density of the RPP composite by more than an order of magnitude (Figure 5b). This would prevent surface relaxation and, in turn, formation of LES, preserving the bulk Wannier exciton. By contrast, RPPs based on an organic cation inducing a larger mismatch, namely, $(4Cl-C_6H_4NH_3)_2PbI_4$ (4Cl-PhA),[27] undergoes increased strain (Figure 5a); thus, larger elastic energy density (Figure 5b) should favor significant (101) surface relaxation suitable for e−h carrier separation.

In summary, surface relaxation effects in layered hybrid perovskite materials have been thoroughly investigated. We introduced the first generic elastic model for LHPs accounting for the internal elastic energy accumulated in the material bulk as a result of lattice mismatch. We show that the mechanical energy is more efficiently relaxed in LHPs thanks to the additional rotational degrees of freedom provided by the perovskite octahedra-based framework. This is further demonstrated using electronic structure calculations of the surface relaxation of perovskite layers in a well-documented family of RPPs, and we discovered a critical layer thickness above which the surface reorganization becomes significant. This consequently leads to the formation of lower energy electronic states rationalizing and confirming experimental observations.[15] Our observation of electronic bandgap shifts and exciton dissociation at the surface, depending on the layered perovskite structure, distinguishes these materials from their 3D $APbI_3$ (A = cation; $n = \infty$) counterparts and pave the way to unique tailored properties and functionalities for optoelectronic, solid-state lighting, or photovoltaic applications.

Methods. DFT calculations are conducted with the SIESTA code.[28] The nonlocal van der Waals density functional of Dion et al. corrected by Cooper (C09) is used for geometry optimizations.[29,30] SOC is taken into account through the on-site approximation as proposed by Fernández-Seivane et al.[31] To prevent conflicts between the on-site treatment and the nonlocality of C09, single point calculations are conducted with the revPBE functional on which C09 is based. The dipole induced in slabs is treated with the dipole correction as implemented in SIESTA.[32] Core electrons are described with

Troullier−Martins pseudopotentials.[33] The valence wave function is developed over a double-ζ polarized basis set of finite-range numerical pseudoatomic orbitals.[34] An energy cutoff of 150 Ry for real-space mesh size is used. Noteworthy, DFT underestimates the bandgap closing upon surface relaxation in RPPs with $n > 2$. Turning to larger supercells, e.g., doubled, is likely to allow for additional distortions, which in turn shall further close the bandgap. Unfortunately, such size doubling is computationally too demanding. Besides, for complex spinor Bloch functions (Kane model) we used the ABINIT package[35] with GGA-revPBE gradient correction for exchange-correlation,[36] ABINIT projector augmented-wave (PAW) data sets[37] as pseudopotentials for Pb, I, and Cs, and an energy cutoff of 19 Ha (517 eV) for the plane-wave basis set. Primitive cells were used for the computation of the electronic band dispersions with Monkhorst−Pack grids for reciprocal space integration of $4 \times 4 \times 1$ for $n = 1$ and $2 \times 2 \times 4$ for $n = 2$, 3, and 4. Spin−orbit coupling was included in all calculations. As plane-wave calculations are more demanding than the localized basis sets counterpart, organic cations have been substituted by Cs atoms. This substitution is known to leave the band dispersion unaffected close to the Fermi level, and in fact, for $n = 3$, we obtain a comparable bandgap closing (128 meV) and similar spinorial components than with SIESTA and all atoms.

■ ASSOCIATED CONTENT

⑤ Supporting Information

The Supporting Information is available free of charge on the ACS Publications website at DOI: 10.1021/acs.nano-lett.8b02078.

> Additional details on the improper flexoelastic model, tilting angles description, construction of the (101) surface, strain energetics, surface band structures and partial electronic densities, Kane models, excitonic properties of RPPs, and references for Figure 5 (PDF)

■ AUTHOR INFORMATION

Corresponding Authors
*E-mail: mikael.kepenekian@univ-rennes1.fr.
*E-mail: serg@lanl.gov.
*E-mail: claudine.katan@univ-rennes1.fr.

ORCID ⓘ
Mikaël Kepenekian: 0000-0001-5192-5896
Boubacar Traore: 0000-0003-0568-4141
Laurent Pedesseau: 0000-0001-9414-8644
Constantinos C. Stoumpos: 0000-0001-8396-9578
Mercouri G. Kanatzidis: 0000-0003-2037-4168
Jacky Even: 0000-0002-4607-3390
Aditya D. Mohite: 0000-0001-8865-409X
Sergei Tretiak: 0000-0001-5547-3647
Claudine Katan: 0000-0002-2017-5823

Notes
The authors declare no competing financial interest.

■ REFERENCES

(1) Zwanenburg, F. A.; Dzurak, A. S.; Morello, A.; Simmons, M. Y.; Hollenberg, L. C. L.; Klimeck, G.; Rogge, S.; Coppersmith, S. N.; Eriksson, M. A. *Rev. Mod. Phys.* **2013**, *85*, 961.

(2) del Alamo, J. A. *Nature* **2011**, *479*, 317−323.

(3) Hwang, H. Y.; Iwasa, Y.; Kawasaki, M.; Keimer, B.; Nagaosa, N.; Tokura, Y. *Nat. Mater.* **2012**, *11*, 103−113.

(4) Haruyama, J.; Sodeyama, K.; Han, L.; Tateyama, Y. *Acc. Chem. Res.* **2016**, *49*, 554−561.

(5) Murali, B.; Yengel, E.; Yang, C.; Peng, W.; Alarousu, E.; Bakr, O. M.; Mohammed, O. F. *ACS Energy Lett.* **2017**, *2*, 846−856.

(6) Saparov, B.; Mitzi, D. B. *Chem. Rev.* **2016**, *116*, 4558−4596.

(7) Pedessdeau, L.; Sapori, D.; Traore, B.; Robles, R.; Fang, H.-H.; Loi, M. A.; Tsai, H.; Nie, W.; Blancon, J.-C.; Neukirch, A. J.; Tretiak, S.; Mohite, A. D.; Katan, C.; Even, J.; Kepenekian, M. *ACS Nano* **2016**, *10*, 9776−9786.

(8) Li, W.; Wang, Z.; Deschler, F.; Gao, S.; Friend, R. H.; Cheetham, A. K. *Nat. Rev. Mater.* **2017**, *2*, 16099.

(9) Tsai, H.; Nie, W.; Blancon, J.-C.; Stoumpos, C. C.; Asadpour, R.; Harutyunyan, B.; Neukirch, A. J.; Verduzco, R.; Crochet, J. J.; Tretiak, S.; et al. *Nature* **2016**, *536*, 312−317.

(10) Mitzi, D. B.; Feild, C. A.; Harrison, W. T. A.; Guloy, A. M. *Nature* **1994**, *369*, 467.

(11) Kagan, C. R.; Mitzi, D. B.; Dimitrakopoulos, C. D. *Science* **1999**, *286*, 945.

(12) Yuan, M.; Quan, L. N.; Comin, R.; Walters, G.; Sabatini, R.; Voznyy, O.; Hoogland, S.; Zhao, Y.; Beauregard, E. M.; Kanjanaboos, P.; Lu, Z.; Kim, D. H.; Sargent, E. H. *Nat. Nanotechnol.* **2016**, *11*, 872−877.

(13) Wang, N.; Cheng, L.; Ge, R.; Zhang, S.; Miao, Y.; Zou, W.; Yi, C.; Sun, Y.; Cao, Y.; Yang, R.; et al. *Nat. Photonics* **2016**, *10*, 699−704.

(14) Odenthal, P.; Talmadge, W.; Gundlach, N.; Wang, R.; Zhang, C.; Sun, D.; Yu, Z.-G.; Vardeny, Z. V.; Li, Y. S. *Nat. Phys.* **2017**, *13*, 894−899.

(15) Blancon, J.-C.; Tsai, H.; Nie, W.; Stoumpos, C. C.; Pedessdeau, L.; Katan, C.; Kepenekian, M.; Soe, C. M. M.; Appavoo, K.; Sfeir, M. Y.; et al. *Science* **2017**, *355*, 1288−1292.

(16) Even, J.; Pedessdeau, L.; Katan, C. *ChemPhysChem* **2014**, *15*, 3733.

(17) Sapori, D.; Kepenekian, M.; Pedessdeau, L.; Katan, C.; Even, J. *Nanoscale* **2016**, *8*, 6369.

(18) Vurgaftman, I.; Meyer, J. R. *J. Appl. Phys.* **2001**, *89*, 5815.

(19) Bimberg, D.; Grundmann, M.; Ledentsov, N. N. *Quantum Dot Heterostructures*; John-Wiley and Sons: 1999.

(20) Ruddlesden, S. N.; Popper, P. *Acta Crystallogr.* **1957**, *10*, 538−539.

(21) Ruddlesden, S. N.; Popper, P. *Acta Crystallogr.* **1958**, *11*, 54−55.

(22) Stoumpos, C. C.; Cao, D. H.; Clark, D. J.; Young, J.; Rondinelli, J. M.; Jang, J. I.; Hupp, J. T.; Kanatzidis, M. G. *Chem. Mater.* **2016**, *28*, 2852−2867.

(23) Davies, J. H.; Bruls, D. M.; Vugs, J. W. A. M.; Koenraad, P. M. *J. Appl. Phys.* **2002**, *91*, 4171−4176.

(24) Blancon, J.-C.; Stier, A. V.; Tsai, H.; Nie, W.; Stoumpos, C. C.; Traore, B.; Pedessdeau, L.; Kepenekian, M.; Tretiak, S.; Crooker, S. A.; et al. *Nat. Commun.* **2018**, *9*, 2254.

(25) Kane, E. O. *Semiconductors and Semimetals*; Academic Press: 1966.

(26) Lemmerer, A.; Billing, D. G. *Dalton Trans.* **2012**, *41*, 1146−1157.

(27) Liu, Z.; Yu, W.-T.; Tao, X.-T.; Jiang, M.-H.; Yang, J.-X.; Wang, L. *Z. Kristallogr. - New Cryst. Struct.* **2004**, *219*, 457−458.

(28) Soler, J. M.; Artacho, E.; Gale, J. D.; García, A.; Junquera, J.; Ordejón, P.; Sánchez-Portal, D. *J. Phys.: Condens. Matter* **2002**, *14*, 2745−2779.

(29) Dion, M.; Rydberg, H.; Schröder, E.; Langreth, D. C.; Lundqvist, B. I. *Phys. Rev. Lett.* **2004**, *92*, 246401.

(30) Cooper, V. R. *Phys. Rev. B: Condens. Matter Mater. Phys.* **2010**, *81*, 161104.

(31) Fernández-Seivane, L.; Oliveira, M. A.; Sanvito, S.; Ferrer, J. *J. Phys.: Condens. Matter* **2006**, *18*, 7999.

(32) Bengtsson, L. *Phys. Rev. B: Condens. Matter Mater. Phys.* **1999**, *59*, 12301.

(33) Troullier, N.; Martins, J. L. *Phys. Rev. B: Condens. Matter Mater. Phys.* **1991**, *43*, 1993−2006.

(34) Artacho, E.; Sánchez-Portal, D.; Ordejón, P.; García, A.; Soler, J. M. *Phys. Status Solidi B* **1999**, *215*, 809−817.

(35) Gonze, X.; Amadon, B.; Anglade, P.-M.; Beuken, J.-M.; Bottin, F.; Boulanger, P.; Bruneval, F.; Caliste, D.; Caracas, R.; Côté, M.; et al. *Comput. Phys. Commun.* **2009**, *180*, 2582−2615.

(36) Zhang, Y.; Yang, W. *Phys. Rev. Lett.* **1998**, *80*, 890.

(37) Torrent, M.; Jollet, F.; Bottin, F.; Zérah, G.; Gonze, X. *Comput. Mater. Sci.* **2008**, *42*, 337−351.